Supplemental Material

to accompany

"Combining micro- and macroscopic probes to untangle single-ion anisotropy and exchange energies in a $S = 1$ quantum antiferromagnet"

Jamie Brambleby[1], Jamie L. Manson[2,3], Paul A. Goddard[1], Matthew B. Stone[4], Roger D. Johnson[5,6], Pascal Manuel[6], Jacqueline A. Villa[2], Craig M. Brown[3], Helen Lu[7], Shalinee Chikara[7], Vivien Zapf[7], Saul H. Lapidus[8], Rebecca Scatena[9], Piero Macchi[9], Yu-sheng Chen[10], Lai-Chin Wu[10] and John Singleton[7]

[1] *Department of Physics, University of Warwick, Gibbet Hill Road, Coventry CV4 7AL, United Kingdom*

[2] *Department of Chemistry and Biochemistry, Eastern Washington University, Cheney, WA 99004, U.S.A.*

[3] *NIST Center for Neutron Research, National Institute of Standards and Technology, Gaithersburg, MD 20899, U.S.A.*

[4] *Quantum Condensed Matter Division, Oak Ridge National Laboratory, Oak Ridge, TN 37831, U.S.A.*

[5] *University of Oxford, Department of Physics, The Clarendon Laboratory, Parks Road, Oxford, OX1 3PU, United Kingdom*

[6] *ISIS Pulsed Neutron Source, STFC Rutherford Appleton Laboratory, Didcot, Oxfordshire OX11 0QX, United Kingdom*

[7] *National High Magnetic Field Laboratory, MS-E536, Los Alamos National Laboratory, Los Alamos, NM 87545, U.S.A.*

[8] *X-ray Sciences Division, Advanced Photon Source, Argonne National Laboratory, Argonne, IL 60439, U.S.A.*

[9] *Department of Chemistry and Biochemistry, University of Bern, 3012 Bern, Switzerland*

[10] *ChemMatCARS, Advanced Photon Source, Argonne National Laboratory, Argonne, IL 60439, U.S.A.*

CONTENTS

A. EXPERIMENTAL METHODS

A1. Design strategy

The tunability offered by metal-organic systems renders them ideal testbeds with which to investigate numerous quantum theories relevant to reduced-dimensionality physics. Our current endeavors are focused on M(II)-based [M = Co ($S = \frac{3}{2}$), Ni ($S = 1$), Cu ($S = \frac{1}{2}$)] coordination polymers, self-assembled from strong charge-assisted H-bonds (*e.g.*, F$\cdots$H$\cdots$F) [1–13]. Weaker O-H$\cdots$F types have also been examined[14–20]. The use of crystal engineering to manage such interactions is a promising path forward in the experimental search for exotic phases of quantum matter. Among the various Ni(II) systems reported thus far, $[Ni(HF_2)(pyz)_2]SbF_6$ (pyz = pyrazine)[3,4], $\alpha-$ and $\beta-$polymorphs of $[Ni(HF_2)(pyz)_2]PF_6$ and $[Ni(HF_2)(3\text{-Clpy})_4]BF_4$ have been synthesized and characterized[1–3,5]. The latter compound forms isolated Q1D Ni—FHF—Ni chains with bent and asymmetric HF_2^- bridges[1,2]. Moreover, the suppressed long-range magnetic order (LRO) and $D/J \approx 1$ are unique to this material, as it is the only Ni(II)-chain proximate to the $D/J = 0.97$ QCP, which separates Haldane, XY-AFM, and QP phases[21].

In $[Ni(HF_2)(pyz)_2]X$, the presence of additional, albeit weak, interchain Ni—pyz—Ni exchange pathways promotes LRO[3–5] below temperatures ≈ 6 K ($X = \alpha-PF_6$), 7 K ($X = \beta-PF_6$), and 12.2 K ($X = SbF_6$). For each compound, a substantial zero-field splitting (ZFS) is also anticipated due to the existing NiN_4F_2 core; *e.g.*, an easy-plane $D = 20$ K has been determined for Q1D $Ni(SiF_6)(vinim)_4$ (vinim = 1-vinylimidazole)[22].

A2. Synthesis

All reagents were obtained from commercial suppliers and used as received. Plasticware was used throughout the entire synthetic process[23]. In a typical synthesis, NiF_2 (1.775 mmol, 302.0 mg) was dissolved separately in 3 mL of aqueous-HF (48-51 % by weight) while NH_4HF_2 (1.775 mmol, 106.5 mg), $LiSbF_6$ (1.775 mmol, 431.8 mg),

TABLE S1. X-ray crystallographic details and refinement results for $[Ni(HF_2)(pyz)_2]SbF_6$. Here, F = amplitude of structure factor of reflection and σ = standard deviation of F. The R-factors are given by $R = \sum |F_{obs} - F_{calc}| / \sum |F_{obs}|$, $R_{int} = \sum |F^2_{obs} - F^2_{calc}| / \sum |F^2_{obs}|$ and $wR = (\sum w|F_{obs} - F_{calc}|^2 / \sum |wFobs|^2)^{\frac{1}{2}}$, where the sums run over all data points and w is a weighting factor. S is the goodness of fit. Errors in parentheses are one standard deviation.

Parameter (units)	
Facility/beamline	Advanced Photon Source/15-ID-B
Chemical formula	$C_8H_9N_4F_8NiSb$
Crystal system	Tetragonal
Space group	$P4/nmm$ (#129; origin choice 2)
Temperature (K)	15(2)
Wavelength, λ (Å)	0.38745
a, b, c (Å)	9.8797(2), 9.8797(2), 6.4292(1)
Volume (Å^3)	627.54(2)
Formula units per unit cell, Z	2
Absorption coefficient, μ (mm^{-1})	1.98
Crystal size (μm$^{3)}$	$10 \times 10 \times 2$
Data collection	
No. of measured reflections [$F > 3\sigma(F)$]	74100
No. of independent reflections	2851
No. of observed reflections	2484
R_{int}	0.0780
Spherical-atom refinement	
R [$F > 3\sigma(F)$], R_{all}, wR, S	0.0318, 0.0427, 0.0612, 1.111
No. parameters	36

TABLE S2. Comparison of selected bond lengths (Å) and bond angles (degrees) for $[Ni(HF_2)(pyz)_2]SbF_6$ as determined by the microcrystal X-ray and neutron powder diffraction studies. Atoms are labelled according to the scheme in Fig.S1. (*Compared to Σ_{vdw} of 2.94 Å for a pair of fluorine atoms.)

	X-rays (T = 15 K)	Neutrons (T = 20 K)	Neutrons (T = 1.5 K)
Ni-N	2.098(1)	2.095(2)	2.096(2)
Ni-F1	2.076(1)	2.067(6)	2.070(6)
H2$\cdots$F1	1.138(1)	1.149(6)	1.146(6)
F1$\cdots$F1*	2.276(1)	2.297(9)	2.292(9)
C-N	1.338(1)	1.338(3)	1.338(3)
C-C	1.391(2)	1.403(3)	1.402(3)
C-H1/D1	0.95	1.071(4)	1.071(4)
Sb-F2	1.869(2)	1.889(4)	1.890(4)
Sb-F3	1.886(1)	1.892(11)	1.893(11)
Sb-F4	1.863(2)	1.771(12)	1.770(13)
Ni$\cdots$Ni (c-axis)	6.4292(1)	6.4319(2)	6.4318(2)
Ni$\cdots$Ni [1 1 0; 1 $\bar{1}$ 0]	6.9860(2)	6.9958(1)	6.9956(1)
F1-Ni-F1	180	180	180
N-Ni-N	90, 180	90, 180	90, 180
F1-Ni-N	90	90	90
Ni-F1$\cdots$H2	180	180	180
Ni-N$\cdots$N	180	180	180
C-N-C	116.97(9)	116.8(3)	116.8(3)
N-C-H1/D1	119.2	119.1(4)	119.0(4)
F2-Sb-F3	89.27(3)	89.8(4)	89.8(5)
F2-Sb-F4	180	180	180
F1-Ni-N-C	73.04(4)	73.7(1)	73.7(1)

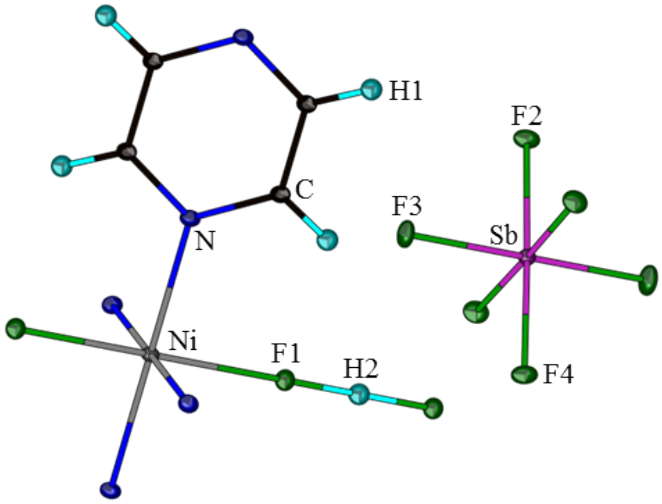

FIG. S1. Structure of $[Ni(HF_2)(pyz)_2]SbF_6$ determined at $T = 15$ K by microcrystal X-ray diffraction. Thermal ellipsoid plot (50 % displacement parameters) showing the basic building blocks and atom-labeling scheme. Ni(II) ions have 4-fold rotational symmetry while the HF_2^- constituent atoms H2 and F1 have respective site symmetries of $\bar{4}m2$ and $2mm$.

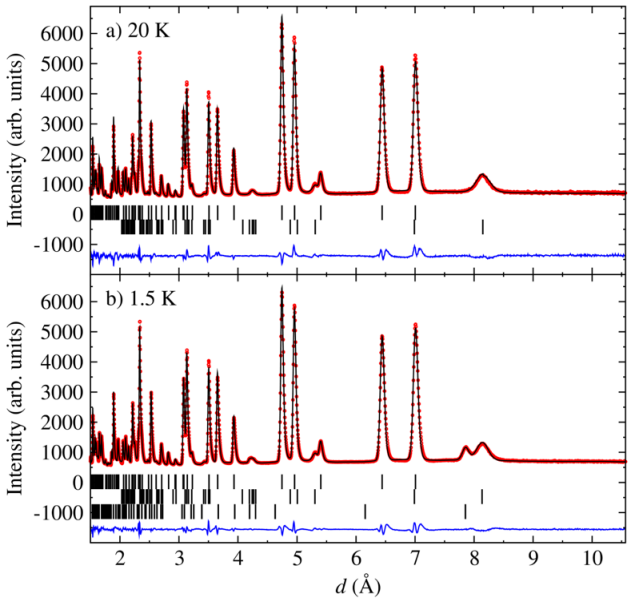

FIG. S2. Refinement of neutron powder diffraction data for $[Ni(HF_2)(pyz\text{-}d_4)_2]SbF_6$ at (a) 20 K and (b) 1.5 K. WISH Bank 2 data (red points), Rietveld fitted model (black line), reflections of the $P4/nmm$ lattice (black ticks, top line), reflections of the magnetic moments with propagation vector $\mathbf{k} = (0, 0, 1/2)$ (black ticks, bottom line) and $I_{obs} - I_{calc}$ (blue line). The bottom row (20 K) and middle row (1.5 K) of ticks in each plot indicate structural peaks due to a 1.6% co-crystallized impurity of $[Ni(pyz)_2(H_2O)_2]FSbF_6$ (orthorhombic; $Ibam$) as determined by LeBail profile matching.

and pyrazine (3.550 mmol, 283.7 mg) were dissolved together in a separate beaker containing 2 mL of aqueous HF and 1 mL H_2O. The NiF_2 solution was slowly mixed with the ligands to give a green solution that was covered with a perforated wax film to allow slow evaporation of the solvent. On standing at room temperature for 3 weeks, a blue powder formed on the bottom and walls of the beaker. The solid was collected by vacuum filtration, washed with 2 mL of H_2O, 2 mL of ethanol, and 2 mL of diethyl ether to assist drying. A pale blue powder, consisting of microcrystalline plates ($10 \times 10 \times 2$ μm^3 in average size), was obtained in high yield (> 80 %, based on Ni(II) content). While these microcrystals were suitable for the synchrotron X-ray structural study they were much too small for single-crystal thermodynamic and neutron-scattering measurements.

For the neutron-scattering experiments, synthesis of a partially deuterated phase of $[Ni(HF_2)(pyz\text{-}d_4)_2]SbF_6$, was necessary to reduce the large incoherent scattering cross-section due to protons (*i.e.* the ^{1}H nuclei). The synthesis was carried out as described above, except pyz was replaced by pyz-d_4. To produce a 1.8 g sample, suitable amounts of HF(aq) and other reagents were used accordingly. X-ray powder diffraction patterns and magnetic susceptibility data were found to be very similar for the hydrogenated and deuterated phases.

A3. Microcrystal X-ray diffraction

Experiments were conducted on the ChemMatCARS 15-ID-B beamline of the Advanced Photon Source (APS) at Argonne National Laboratory (ANL). A microcrystal of $[Ni(HF_2)(pyz)_2]SbF_6$ measuring $10 \times 10 \times 2$ μm^3 was selected from a bulk sample using a cryo-loop and mounted on a Bruker D8 fixed-chi X-ray diffractometer equipped with an APEX II CCD area detector. The sample was cooled to 15(2) K using a He-cryojet. Synchrotron radiation with a beam energy of 32.2 keV ($\lambda = 0.38745$ Å) was used, and the beam size at the sample was 0.1×0.1 mm^2. The distance between sample and detector was set at 60 mm. A total of 720 frames were collected at $\theta = -5°, 140°$ and 180° with the ϕ-angle scanned over 180° at intervals of 0.5°. Data collection and integration were performed using the APEX II software suite. Data reduction employed SAINT[24]. Resulting intensities were corrected for absorption by Gaussian integration (SADABS)[25]. The structural solution (XT) [26] and refinement (XL) [27] were carried out with SHELX software using the XPREP utility for the space-group determination. Considering systematic absences, the crystal structure was solved in the tetragonal space group $P4/nmm$ (#129, origin choice 2) [28]. Pyrazine H-atoms were placed in idealized positions and allowed to ride on the carbon atom to which they are attached. All non-hydrogen atoms were refined with anisotropic thermal displacement parameters. The atom-labelling scheme is shown in Fig. S1. Full details of the structural refinement are given in Table S1, while Table S2 shows selected bond

TABLE S3. Refinement details from neutron powder-diffraction data for $[Ni(HF_2)(pyz\text{-}d_4)_2]SbF_6$ at 1.5 K and 20 K. The magnetic propagation vector in reciprocal lattice units (r.l.u.) is k and μ is the refined Ni(II) magnetic moment. The goodness-of-fit parameters $R_F = \sum |I_{obs}^{\frac{1}{2}} - I_{calc}^{\frac{1}{2}}| / \sum I_{obs}^{\frac{1}{2}}$, $R_{Bragg} = \sum |I_{obs} - I_{calc}| / \sum |I_{obs}|$, where I_{obs} is the observed intensity, I_{calc} is the calculated intensity and the sum runs over all data points. R_{mag} is the equivalent R factor to R_{Bragg} applied to the fit of the magnetic scattering only.

Parameter (units)		
Formula	$C_8HD_8N_4F_8NiSb$	$C_8HD_8N_4F_8NiSb$
Temperature (K)	20	1.5
Space group	$P4/nmm$	$P4/nmm$
a, b, c (Å)	9.8936(1), 9.8936(1), 6.4319(2)	9.8933(1), 9.8933(1), 6.4318(2)
Volume (Å^3)	629.57(2)	629.53(2)
Z	2	2
k (r.l.u.)	–	(0, 0, 1/2)
Order type	–	G-type
$\mu(\mu_B)$	–	2.03(7)
WISH detector banks	Bank 2 + Bank 9	Bank 2 + Bank 9
R_F (%)	5.42	5.46
R_{Bragg} (%)	3.64	3.62
R_{mag} (%)	–	5.89 ($m \perp c$), 18.6 ($m \parallel c$)

lengths and angles.

A4. Elastic neutron scattering

Magnetic diffraction patterns were recorded on the WISH diffractometer (ISIS, Rutherford Appleton Laboratory, UK)[29]. As mentioned above, a partially deuterated sample, $[Ni(HF_2)(pyz\text{-}d_4)_2]SbF_6$, of mass 1.8 g was loaded into a cylindrical vanadium can and placed in an Oxford Instruments cryostat with a base temperature of 1.5 K. Diffraction data were collected over the temperature interval $1.5 - 20$ K, with long counting times (8 hrs) at 1.5 K and 20 K. Intermediate temperature points were measured with an exposure time of 2 hrs. Rietveld refinements were performed using FULLPROF[30]. All atoms were refined using isotropic thermal displacement parameters. Figure S2 shows the refinement of the neutron powder diffraction data. A description of the results of the refinement is included in the main text. Unit-cell parameters derived from neutron scattering can be found in Table S2, whereas Table S3 compares bond lengths and bond angles provided by the X-ray and neutron experiments. Table S4 compares the observed and calculated magnetic structure factors.

A5. Heat capacity

Heat capacity (C_p) measurements were carried out using a 9 T Quantum Design PPMS, with a 1.91(5) mg powder sample of $[Ni(HF_2)(pyz)_2]SbF_6$ that was pressed into a pellet, secured to a sapphire stage with Apiezon-N grease and held in contact with a large thermal bath. Measurements of C_p were performed using the traditional relaxation method[31]. For this technique, a heat pulse

TABLE S4. Observed and calculated magnetic structure factors for $[Ni(HF_2)(pyz)_2]SbF_6$ as determined by the 1.5 K neutron-diffraction study. F_o and F_c correspond to observed and calculated values, respectively, for a given d-spacing.

h	k	l	F_o^2	F_c^2 ($\perp c$)	F_c^2 ($\parallel c$)	d-spacing (Å)
1	0	$\frac{3}{2}$	2.999	2.927	0.431	3.9358
1	2	$\frac{1}{2}$	3.539	3.662	5.079	4.1856
1	0	$\frac{1}{2}$	2.631	2.854	2.241	7.8454

TABLE S5. Fitted parameters for the phonon heat capacity of $[M(HF_2)(pyz)_2SbF_6$, where M = Ni(II), Cu(II) [10] and Co(II) [6]. The simplest lattice model[10] required to fit the data included one Debye (D) and two Einstein (E) modes that are each determined by an amplitude (A_i) and characteristic temperature (θ_i) (i =D, E).

	Ni(II)	Cu(II)	Co(II)
A_D (JK^{-1}mol^{-1})	123(3)	76(1)	82(1)
θ_D (K)	148(3)	94(8)	80(1)
A_{E1} (JK^{-1}mol^{-1})	271(6)	134(4)	174(3)
θ_{E1} (K)	345(7)	208(4)	177(2)
A_{E2} (JK^{-1}mol^{-1})	240(6)	191(4)	287(3)
θ_{E2} (K)	860(30)	500(3)	448(6)

(≈ 1 % of the thermal bath temperature) was applied to the stage and C_p evaluated by measuring the time constant of the thermal decay curve. The heat capacities of the Apiezon-N grease and sample platform were measured separately and subtracted from the total to obtain the heat capacity of the sample. The data for $T \geq 32$ K were modeled[10] with one Debye and two Einstein phonon modes and the resulting fit parameters are tabulated in

TABLE S6. Coefficients (c_{ij}, Eqn. S2) for the polynomials (a_i, Eqn. S1) from Ref. 32.

Polynomial (a_i)	c_{i0}	c_{i1}	c_{i2}
$i = 0$	1.67268034	-0.26449121	-0.102945
$i = 1$	1.710151691	0.5114739	0.18853874
$i = 2$	1.899474528	-0.166396406	0.1494167
$i = 3$	1	0	0

Table S5. The fitted data are shown in the main text.

A6. Temperature-dependent linear susceptibility

Linear susceptibility ($M/\mu_0 H$, where M is the magnetization) measurements were made for temperatures in the range $1.9 \leq T \leq 50$ K and fields $\mu_0 H \leq 13$ T using a Quantum Design Physical Property Measurement System (PPMS) equipped with a vibrating sample magnetometer (VSM). A 2 mg powder sample was loaded into a brass holder, and mounted in the VSM transport. The sample was initially cooled in zero applied field to $T = 1.9$ K. Data were collected upon warming and corrected for diamagnetic contributions from the sample and background.

As described in the main text, the susceptibility data for $T \geq 10$ K are compared to a simulation of the susceptibility ($\chi_{\rm sim}$) using a 1D chain model of Borrás-Almenar *et al.*[32]. This applies to chains of $S = 1$ ions with intrachain exchange J and single-ion anisotropy D, and is expressed as:

$$\chi_{\rm sim} = \frac{2\mu_0 N_{\rm A} \mu_{\rm B}^2 g^2}{3 k_{\rm B} J} \left[\frac{t^2 + 0.5t + 0.1}{a_3 t^3 + a_2 t^2 + a_1 t + a_0} \right] \quad \text{(S1)}$$

where $t = \frac{T}{J}$ is the reduced temperature and the coefficients a_i are polynomials of the $\frac{D}{J}$ ratio:

$$a_i = \sum_{j=0}^{2} c_{ij} \left(\frac{D}{J} \right)^j \quad \text{(S2)}$$

with the coefficients c_{ij} given in Table S6. Eqn. S1 can be used to attempt fits of $\chi(T)$ data for powders.

A7. Pulsed-field magnetization

Measurements of the powder magnetization of $[Ni(HF_2)(pyz)_2]SbF_6$ up to 60 T made use of a 1.5 mm bore, 1.5 mm long, 1500-turn compensated-coil susceptometer, constructed from a 50 gauge high-purity copper wire[9]. When the sample is within the coil, the signal voltage V is proportional to $\mathrm{d}M/\mathrm{d}t$, where t is time. Numerical integration of V is used to evaluate M. The sample is mounted within a 1.3 mm diameter ampoule that can be moved in and out of the coil. Accurate values of M are obtained by subtracting empty-coil data from that measured under identical conditions with the sample present. The susceptometer was placed inside a ^{3}He cryostat providing a base temperature of 0.5 K. The magnetic field was measured by integrating the voltage induced in a 10-turn coil calibrated by observing the de Haas-van Alphen oscillations of the belly orbits of the copper contained in the susceptometer coil[9].

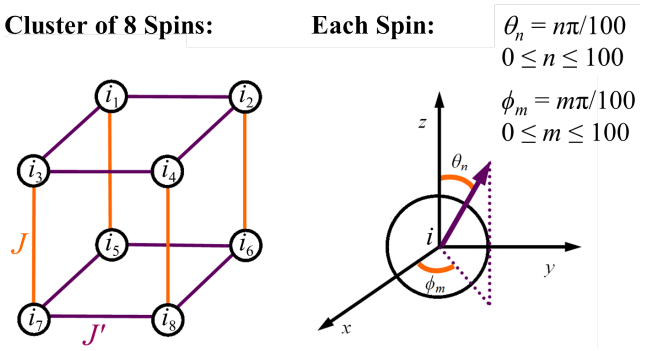

FIG. S3. The 2×2 planar arrangement of Ni(II) ions used in the simulation of the magnetization. Each ion (i) is represented by a vector where the two degrees of freedom are the polar angles θ_n and ϕ_m, each limited to 100 evenly spaced values. J and J' correspond to Ni—FHF—Ni and Ni—pyz—Ni exchange interactions, respectively.

A8. Inelastic neutron scattering

Two INS measurements were performed using the disk-chopper spectrometer (DCS) located at the NIST Center for Neutron Research (NCNR)[33]. Both measurements used neutrons of wavelength 3.7 Å to scatter from a 1.8 g, partially deuterated powder sample of $[Ni(HF_2)(pyz\text{-}d_4)_2]SbF_6$ loaded in an aluminum sample can sealed under a helium atmosphere. The first measurement was conducted in zero field to probe the temperature-dependence of INS spectra at $T = 1.6$ K, 10 K, and 20 K. The magnetic spin excitations were examined by subtracting the 20 K (*i.e.* above the ordering temperature) data from the 1.6 K measurement.

Thermodynamic parameters were determined by comparing the measured powder spin-wave spectra against a series of spectra simulated using the SPINW analysis package[34], assuming the XY magnetic structure determined by elastic neutron scattering. The second measurement surveyed the magnetic-field dependence of spin excitations at $T = 1.6$ K and 20 K in magnetic fields of $\mu_0 H = 0, 3, 6$, and 10 T. To account for the time-independent background of the measurements, an overall value of 27 counts per hour per detector was subtracted from the data. This value was not subtracted in cases where data are plotted as the difference between two temperatures or two fields.

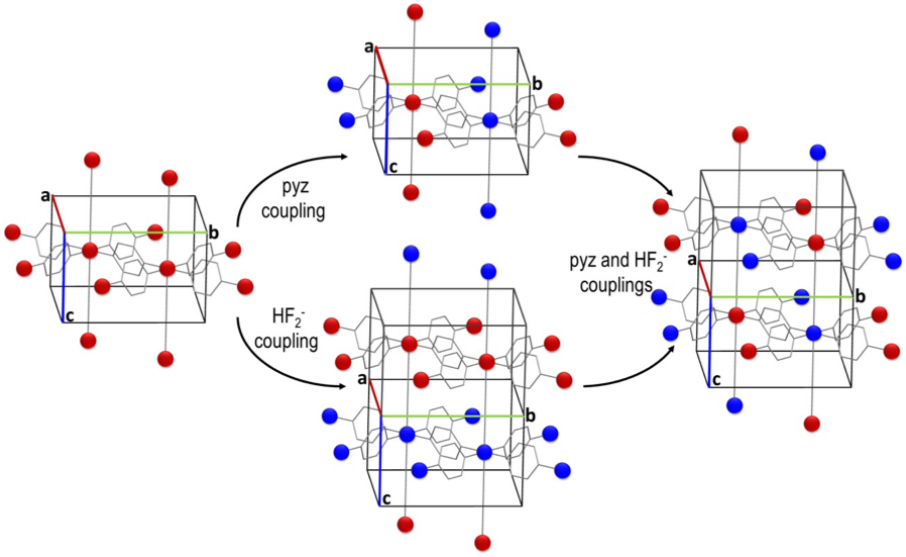

FIG. S4. Models used in the DFT calculation of the J and J' exchange interactions. We consider an FM state and two different AFM states, with spin pairing along the c-axis (AFM_{FHF}) or in the ab-plane (AFM_{pyz}), as well as the fully AFM state featuring both kinds of pairing.

B. THEORY, CALCULATIONS AND SIMULATIONS

B1. Monte-Carlo simulation of high-field magnetization

We compute the powder-average magnetization of $[Ni(HF_2)(pyz)_2]SbF_6$ using a classical Monte-Carlo routine written in MATLAB[35]. A cluster of 8 ions is arranged in two sets of 2×2 planes (Fig. S3) and the magnetic moment of each ion (i) is represented by a classical vector, constrained by the polar angles θ_i and ϕ_i. The spins are coupled via the Hamiltonian of Eqn. 1 (main text), for which periodic boundary conditions are applied. The zero-field spin configuration uses the results of elastic neutron scattering starting with collinear moments, antiferromagnetically coupled to all neighbors and oriented within the $xy-$planes. The simulation considered how the lowest-energy configuration of spins changes in a magnetic field. This was repeated for twenty-one evenly spaced angles (α) between the magnetic field and the hard-axis (z) and for values in the range $0 \leq \alpha \leq 180°$.

For a fixed value of α, the magnitude of the field is increased from 0 to 60 T in $\mu_0 \Delta H = 0.3$ T steps. Following the field increment, the energy of the cluster was minimized with respect to the angles (θ_n, ϕ_m) using the Metropolis Monte Carlo algorithm[36]. First, θ for one spin is changed to a new random value and the energy of the new configuration calculated from Eqn. 1 (main text). If the energy decreases, the change is accepted. If the energy is raised by an amount ΔE, the change is accepted with a probability $\exp(-\Delta E/k_B T)$, otherwise the move is rejected. Next, the reorientation of the angle ϕ of the spin is considered in the same way as before applying the routine to the remaining seven moments in the cluster. This process is repeated 2000 times for a particular value of magnetic field. Once complete, the magnetization parallel to the applied field, $\mathbf{M}(\alpha, \mathbf{H}).\frac{\mathbf{H}}{|\mathbf{H}|}$, was extracted and recorded. The powder average magnetization at a particular magnetic field, $M_{avg}(H)$, is then determined by

$$M_{avg}(H) = \frac{\sum_\alpha \left[\mathbf{M}(\alpha, \mathbf{H}).\frac{\mathbf{H}}{|\mathbf{H}|}\right] \sin\alpha \Delta\alpha}{\sum_\alpha \sin\alpha \Delta\alpha} \qquad \text{(S3)}$$

Owing to the condition which allows the energy to be raised during a field step, the final spin configuration will be within an energy of $k_B T$ from the true ground state. Hence, the parameter T plays the role of temperature. Here, T is chosen to be 0.1 K, so as to find the most probable ground state spin configuration.

B2. DFT calculation of spin density

The exchange-coupling constant J can be related to the energy difference between states with different spin multiplicities[37–40]. For this purpose, accurate unrestricted wave functions for the ferromagnetic (FM) and AFM spin states are required. We have investigated the FM and several combinations of AFM states, imposing a coupling only along Ni—FHF—Ni or the Ni—pyz—Ni directions, or along both, in order to estimate J and J' as well as the total coupling. The methodology is illustrated in the schematic shown in Fig. S4.

The CRYSTAL14 code[41] was used to perform DFT calculations with periodic boundary conditions on rele-

vant FM and AFM phases of $[Ni(HF_2)(pyz)_2]SbF_6$ using the B3LYP hybrid functional. The basis set was $6-31G(d,p)$ [42] for all of the atoms except for Sb which utilized $3-21G(d)$ [43]. Electron-spin and charge-density maps were calculated using the routines in CRYSTAL14 and the spin-atomic distribution was determined using Mulliken partitioning[44].

C. EXCHANGE INTERACTION STRENGTHS IN RELATED COMPOUNDS

TABLE S7. Review of the exchange interaction strengths mediated through Ni-pyz-Ni linkages (J') for coordination polymers consisting of approximately square $[Ni(pyz)_2]^{2+}$ plaquettes similar to those found in $[Ni(HF_2)(pyz)_2]SbF_6$. The values listed were obtained by thermodynamic measurements.

System	J' (K)	T_c (K)	Ref.
$NiCl_2(pyz)_2$	0.49(1)	< 0.08	45
$NiBr_2(pyz)_2$	1.00(5)	1.8(1)	45
$NiI_2(pyz)_2$	< 1.19	2.5(1)	45
$Ni(NCS)_2(pyz)_2$	0.82(5)	1.8(1)	45
$[Ni(H_2O)_2(pyz)_2](BF_4)_2$	1.05(5)	3.0(1)	46

[1] J.L. Manson, A.G. Baldwin, B.L. Scott, J. Bendix, R.E. Del Sesto, P.A. Goddard, Y. Kohama, H.E. Tran, S. Ghannadzadeh, J. Singleton, T. Lancaster, J.S. Möller, S.J. Blundell, F.L. Pratt, V.S. Zapf, J. Kang, C. Lee, M.-H. Whangbo, C. Baines, Inorg. Chem. **51**, 7520 (2012).

[2] J.-S. Xia, A. Ozarowski, P.M. Spurgeon, A.C. Baldwin, J.L. Manson, M.W. Meisel, arXiv:1409.5971 (2014).

[3] J.L. Manson, S.H. Lapidus, P.W. Stephens, P.K. Peterson, K.E. Carreiro, H.I. Southerland, T. Lancaster, S.J. Blundell, A.J. Steele, P.A. Goddard, F.L. Pratt, J. Singleton, Y. Kohama, R.D. McDonald, R.E. Del Sesto, N.A. Smith, J. Bendix, S.A. Zvyagin, J. Kang, C. Lee, M.-H. Whangbo, V.S. Zapf, A. Plonczak, Inorg. Chem. **50**, 5990 (2011).

[4] K.R. O'Neal, B.S. Holinsworth, Z. Chen, P.K. Peterson K.E. Carreiro, C. Lee, J.L. Manson, M.-H. Whangbo, Z. Li, Z. Liu and J.L. Musfeldt, Inorg. Chem. **55** 12172 (2016).

[5] J.L. Manson, K.E. Carreiro, S.H. Lapidus, P.W. Stephens, P.A. Goddard, R.E. Del Sesto, J. Bendix, S. Ghannadzadeh, I. Franke, J. Singleton, T. Lancaster, J.S. Möller, P.J. Baker, F.L. Pratt, S.J. Blundell, J. Kang, C. Lee, M.-H. Whangbo, Dalton Trans. 2012, **41**, 7235 (2012).

[6] J. Brambleby, P.A. Goddard, R.D. Johnson, J. Liu, D. Kaminski, A. Ardavan, A.J. Steele, S.J. Blundell, T. Lancaster, P. Manuel, P.J. Baker, J. Singleton, S. Schwalbe, P.M. Spurgeon, H.E. Tran, P.K. Peterson, J.F. Corbey, J.L. Manson, Phys. Rev. B **92**, 134406 (2015).

[7] J.L. Manson, M.M. Conner, J.A. Schlueter, T. Lancaster, S.J. Blundell, M.L. Brooks, F.L. Pratt, T. Papageorgiou, A.D. Bianchi, J. Wosnitza, M.-H. Whango, Chem. Commun. **2006**, 4894 (2006).

[8] J.L. Manson, H.I. Southerland, B. Twamley, R. Rai, J.L. Musfeldt, Dalton Trans. **2007**, 5655 (2007).

[9] P.A. Goddard, J. Singleton, P. Sengupta, R.D. McDonald, T. Lancaster, S.J. Blundell, F.L. Pratt, S. Cox, N. Harrison, J.L. Manson, H.I. Southerland, J.A. Schlueter, New J. Phys. **10**, 083025 (2008).

[10] J.L. Manson, J.A. Schlueter, K.A. Funk. H.I. Southerland, B. Twamley, T. Lancaster, S.J. Blundell, P.J. Baker, F.L. Pratt, J. Singleton, R.D. McDonald, P.A. Goddard, P. Sengupta, C.D. Batista, L. Ding, C. Lee, M.-H. Whangbo, I. Franke, S. Cox, C. Baines, D. Trial, J. Amer. Chem. Soc. **131**, 6733 (2009).

[11] E. Čižmár, S.A. Zvyagin, R. Beyer, M. Uhlarz, M. Ozerov, Y. Skourski, J.L. Manson, J.A. Schlueter, J. Wosnitza, Phys. Rev. B **81**, 064422 (2010).

[12] J.L. Manson, M.L. Warter, J.A. Schlueter, T. Lancaster, A.J. Steele, S.J. Blundell, F.L. Pratt, J. Singleton, R.D. McDonald, C. Lee, M.-H. Whangbo, A. Plonczak, Angew. Chem. Int. Ed. **50**, 1573 (2011).

[13] W. Li, M.S.R.N. Kiran, J.L. Manson, J.A. Schlueter, A. Thirumurugan, U. Ramamurty, A.K. Cheetham, Chem. Commun. **49**, 4471 (2013).

[14] S.H. Lapidus, J.L. Manson, H. Park, A.J. Clement, S. Ghannadzadeh, P.A. Goddard, T. Lancaster, J.S. Möller, S.J. Blundell, M.T.F. Telling, J. Kang, M.-H. Whangbo, J.A. Schlueter, Chem. Commun. **49** 499 (2013).

[15] S. Ghannadzadeh, J.S. Möller, P.A. Goddard, T. Lancaster, F. Xiao, S.J. Blundell, A. Maisuradze, R.

Khasanov, J.L. Manson, S.W. Tozer, D. Graf, J.A. Schlueter, Phys. Rev. B 2013, **87**, 241102R (2013).
[16] C.H. Wang. M.D. Lumsden, R.S. Fishman, G. Ehlers, T. Hong, W. Tian, H. Cao, A. Podlesnyak, C. Dunmars, J.A. Schlueter, J.L. Manson, A.D. Christianson, Phys. Rev. B **86**, 064439 (2012).
[17] A. Prescimone, C. Morien, D. Allan, J.A. Schlueter, S.W. Tozer, J.L. Manson, S. Parsons, E.K. Brechin, S. Hill, Angew. Chem. Int. Ed. **51**, 7490 (2012).
[18] G.J. Halder, K.W. Chapman, J.A. Schlueter, J.L. Manson, Angew. Chem. Int. Ed. **50**, 419 (2011).
[19] J.L. Musfeldt, Z. Liu, S. Li, J. Kang, C. Lee, P. Jena, J.L. Manson, J.A. Schlueter, G.L. Carr, M.-H. Whangbo, Inorg. Chem. **50**, 6347 (2011).
[20] J.L Manson, M.M. Conner, J.A. Schlueter, A.C. McConnell, H.I. Southerland, I. Malfant, T. Lancaster, S.J. Blundell, M.L. Brooks, F.L. Pratt, J. Singleton, R.D. McDonald, C. Lee, M.-H. Whangbo, Chem. Mater. **20**, 7408 (2008).
[21] K. Wierschem, P. Sengupta Mod. Phys. Lett. B **28**, 1430017 (2014) and refs. therein.
[22] J.L. Manson, A. Ozarowski, S.H. Lapidus, J.A. Villa, A. Sarkar, S. Saeidi, M.W. Meisel, preprint (2016).
[23] Caution! Hydrofluoric acid must be handled with great care as it is highly toxic, corrosive, and will cause severe burns. Proper personal protective equipment must be worn at all times regardless of the amount of HF being used.
[24] SAINT v8.34A; Bruker AXS Inc.: Madison, WI, 2013
[25] SADABS v.2014/15; Bruker AXS Inc.: Madison, WI, 2014
[26] SHELXT v.2014/4; Bruker AXS Inc.: Madison, WI, 2014
[27] SHELXL v.2014/7; Bruker AXS Inc.: Madison, WI, 2014
[28] International Tables for Crystallography (2006). Vol. A, part 7, pp. 448-449.
[29] L. Chapon, P. Manuel, P.Radaelli, C. Benson, L. Penot, S. Ansell, N. Rhodes, D. Raspino, D. Duxbury, E. Spill, J, Norris, Neutron News **22**, 22 (2011).
[30] J. Rodriguez-Carvajal, Physica (Amsterdam) **192**, 55 (1993).
[31] J. Lashley, M.F. Hundley, A. Migliori, J.L. Sarrao, P.G. Pagliuso, T.W. Darling, M. Jaime, J.C. Cooley, W.L. Hults, L. Morales, D. Thoma, J.L. Smith, J. Boerio-Goates, B.F. Woodfield, G.R. Stewart, R.A. Fisher, N.E. Phillips, Cryogenics **43**, 369 (2003).
[32] J.J. Borrás-Almenar, E. Coronado, J. Curely, R. Georges, Inorg. Chem. **34**, 2699 (1995).
[33] J. Copley, Physica B **180-181**, 914 (1992).
[34] S. Toth, B. Lake, J. Phys. Condens. Matter **27**, 166002 (2015).
[35] MATLAB v.8.0.0.783; The Math Works, Inc.: Natick, MA, 2012
[36] D.P. Landau, K. Binder, *A Guide to Monte Carlo Simulations in Statistical Physics*, 3rd Ed.; (Cambridge University Press, Cambridge, 2009) pp. 68-137.
[37] L.J. Noodleman, Chem. Phys. **74**, 5737 (1981).
[38] L.J. Noodleman, E.R. Davidson, Chem. Phys. **109**, 131 (1986).
[39] M. Deumal, M.J. Bearpark, J.J. Novoa, M.A. Robb, J. Phys. Chem. A **106**, 1299 (2002).
[40] E. Ruiz, J. Cano, S. Alvarez, P.J. Alemany, J. Comput. Chem. **20**, 1391 (1999).
[41] R. Dovesi, V.R. Saunders, C. Roetti, R. Orlando, C.M. Zicovich-Wilson, F. Pascale, B. Civalleri, K. Doll, N.M. Harrison, I.J. Bush, P. DArco, M. Llunell, M. Causà, Y. Noël, CRYSTAL14 Users Manual. (University of Torino, Torino 2014).
[42] P.C. Hariharan, J.A. Pople, Theor. Chim. Acta **28**, 213 (1973).
[43] K.D. Dobbs, W.J. Hehre, J. Comput. Chem. **8**, 880 (1987).
[44] R.S. Mulliken, J. Chem. Phys. **23**, 1833 (1955).
[45] J. Liu, P.A. Goddard, J. Singleton, J. Brambleby, F. Foronda, J.S. Möller, Y. Kohama, S. Ghannadzadeh, A. Ardavan, S.J. Blundell, T. Lancaster, F. Xiao, R.C. Williams, F.L. Pratt, P.J. Baker, K. Wierschem, S.H. Lapidus, K.H. Stone, P.W. Stephens, J. Bendix, M.R. Lees, T.J. Woods, K.E. Carreiro, H.E. Tran, C.J. Villa, J.L. Manson, Inorg. Chem. **55**, 3515 (2016); and unpublished results.
[46] W.J.A. Blackmore, J. Brambleby, P.A. Goddard, M. Healey, B. Slater, J. Singleton, A. Ozarowski, J.A. Schlueter, S.H. Lapidus, J.A. Villa, D.Y. Villa, J.L. Manson, in preparation (2017).